Elastoplastic response and recoil of honeycomb lattices

Alessandra Bonfanti[a,b], Atul Bhaskar[b]

[a] *Department of Engineering, University of Cambridge, Cambridge, CB2 1PZ, UK*
[b] *Faculty of Engineering and the Environment, Boldrewood Innovation Campus, University of Southampton, SO16 7QF, Southampton, UK*

Abstract

This paper presents elasto-plastic response and recoil analysis of two-dimensional honeycombs. The architecture studied here possesses cell wall bending as the dominant mechanism of deformation. Elasto-plastic analysis of cell walls, in conjunction with the kinematics of the deformation of the lattice, enables us to obtain closed form plastic response as well as recoil upon unloading. Elastic-perfectly plastic cell wall material is considered. A smooth apparent structural response is observed although the material model is piece-wise linear. The apparent Poisson's ratio of the porous honeycomb material, in the plastic regime, is derived from the lateral response calculation. In the non-linear regime of deformation, the Poisson's ratio of honeycombs remains independent of the apparent strain of the lattice. A parametric study of the non-linear response involving systematic changes in the parameters is carried out. This suggests the existence of non-dimensional groups that could provide response relationship valid for all geometric and material parameters. Scaling arguments are developed and a scaling ansatz is proposed which leads to data collapse, based upon which, a family of honeycombs can be *analytically* characterised for elasto-plastic response. Data collapse thus obtained provides a master-curve for structure-property relationship for plasticity of honeycombs which separates the individual cell wall mechanics from the lattice kinematics.

Keywords: Lattice material, Spring back, plastic analysis

1. Introduction

Materials with lattice architecture at the mesoscopic length scales are frequently used in engineering. For example, sandwich constructions in aeronautical applications frequently use honeycombs in their core, designed to resist shear deformation. Materials such as those used in electromechanical sensors, automotive catalytic converters, impact and sound absorption devices [1, 2] frequently make use of the cellular and porous internal geometry to achieve specific functions. Biomaterials and scaffolds often possess lattice geometry to allow cell proliferation and growth in addition to providing the mechanical stiffness and strength of the implant during their deployment and service. More recently, with the advent of acoustic meta-material, the promise of tailoring acoustic waves has opened new possibilities in the area of structured materials. Interestingly, the mechanical properties achieved by lattice materials are frequently superior to those of the corresponding constituent solid [1] and this is achieved by placing material where it is needed. For many applications, elastic analysis alone is not sufficient. For example, material for energy absorption and the performance of biomedical implants such as cardiovascular stent require detailed elasto-plastic response and springback calculations. Stents are cellular scaffolds that are expanded during surgery to the post-plastic state in order to open blocked blood vessels permanently. Further, a quantitative prediction of recoil is also required in this context because one needs to know the post-ballooning diameter of the stents. Helmets and sport protections are often made of lattice structures, because of their energy absorption capability. Their core is designed to accommodate plastic deformation when subjected to heavy loadings [3]. Due to the wide applicability of such lattice material and periodic structures, a sound understanding of their mechanical behaviour is critical for their design.

When lattice materials are remotely loaded in tension, the response is initially linear which is followed by plastic deformations. Once the load is removed, the elastic deformation is recovered whilst the deformation associated with the plastic behaviour is permanent. This is known as elastic recoil or spring back.

The calculation of linear elastic response and collapse analysis using plastic hinge theory for hexagonal honeycombs was provided by Gibson and Ashby [1]. Linear elastic analysis was extended to geometrically non-linear behaviour at large deformations by Hu and *et al.* [4]. Following the seminal work of Gibson and Ashby [1], a large body of literature on the linear mechanics and engineering of cellular materials has appeared. This includes the investigation of the role of the nodes at the intersection of the inclined and vertical members on the elastic properties [5], in addition to experimental work in the area of impact and crushing [6, 7]. Further, buckling instability of such honeycombs under compressive loading has been studied by Haghpanah et al. [8]. The mechanics of spring back has been extensively explored previously to model metal forming processes. However, it has not been studied yet in the field of architectured materials, since it firstly requires the determination of the complete nonlinear lattice response after yielding. A detailed elasto-plastic analysis followed by recoil upon unloading seems to be missing in the literature. The present work fills the gap between the known results for elastic response and the collapse limit via the intermediate stages of non-linear plastic response. The apparent Young's modulus and Poisson's ratio fully characterise the elastic response of lattice structures. For the non-linear apparent elasto-plastic response, we need the complete stress-strain relationship. A regular hexagonal honeycomb geometry has been considered here in order to facilitate analytical calculations and also to provide a benchmark solution for future development in the area.

The lattice geometry considered here lends itself to bending dominance and formation of plastic hinges upon loading which manifests into desirable properties such as energy absorption capability [9, 10]. The hexagonal honeycomb is one of the most frequently studied configurations over the years in the cellular materials field. A reason for this is the potential applicability of the results obtained from regular hexagonal honeycombs to other cellular structures that exhibit bending dominance. Methods have been developed previously to analyse honeycombs when they deform elastically. In the early 1980s, Abd El-Sayed *et al.* [11] studied hexagonal honeycombs analytically by using beam theory to

model the cell walls. They calculated the in-plane Young's moduli, Poisson's ratio and the plastic collapse load. The geometry that they considered has cell walls of double thickness parallel to one direction than the other two. Gibson and Ashby [1] considered a hexagonal lattice with identical cell walls which leads to isotropic bulk behaviour for regular hexagonal honeycombs. They used a unit cell approach informally and derived apparent linear elastic properties there from. The use of a repetitive unit in large numbers helps the manufacture of this class of materials and structures [12, 13] that possess translational symmetry. Theoretically, translational symmetry inherent in the geometry facilitates closed form analysis. In the present work, we make use of this periodicity in order to be able to analytically calculate the response during loading and unloading of such lattice material past the yield. The material considered is elastic-perfectly plastic, which is a frequently used idealisation in analytical work.

The plastic limit behaviour of cellular material subjected to in-plane compressive load has been extensively studied in the past using a combination of experimental and analytical approaches. When subjected to compression, the failure of the lattice can be due to elastic buckling or plastic collapse of the struts. Gibson and Ashby [1] used the plastic hinge theory to obtain the collapse limit of honeycombs. This approach is based on the mechanics of cell collapse, when the moment in a cell wall equals the fully-plastic moment of the cross section. Menges and Knipschild [14] estimated the 'elastic' failure stress by assuming that the collapse of the cells corresponds to the buckling of the struts. However, such approach greatly overestimates the failure stress for crushed honeycombs [15]. Klintworth and Stronge [15] combined elastic buckling modes and plastic collapse modes, that are geometrically similar, to obtain the elasto-plastic crushing modes of honeycomb. Taking into account the interaction between these two phenomena allowed a more accurate estimation of the collapse stress. Before the fully plastic moment within a section of a strut is reached, the cell walls start to deform plastically, if buckling does not occur. An analysis of this process is missing in the Klintworth and Stronge model [15]. Zhu and Mills [16]

studied the effects of the material parameters on the elastic and plastic collapse of honeycombs with different relative densities. Three plastic collapse modes are found by Karagiozova and Yu [17] in the deformation of regular hexagonal honeycombs. By using the plastic hinge theory, they studied the preferable deformation mode under prescribed loading conditions based on the principle of the lowest internal energy. Chuang and Huang [18] studied the yield surface for an hexagonal honeycombs with plateau borders using the plastic hinge theory. They presented the combination of loading at which the material within the struts reaches its yield point. This was further extended for five other types of cell configurations by Wang and McDowell [19]. Crushing of honeycombs has been experimentally studied by Papka *et al.* [20] in order to examine the three regimes that honeycombs show during compression–linear, plateau and densification regions. Such experimental results were compared with numerical simulations, which gave a higher stiffness and plateau stress. This can be due to geometric imperfections arising during the manufacturing process of honeycombs. Some years later, the same authors studied in-depth the influence of imperfections on the mechanical properties of honeycombs [21]. Using numerical simulation, Chen *et al.* [22] brought out the effect of defects on the hydrostatic yield strength of foams. A numerical study of plastic deformation of a honeycomb and Voronoi structures has been performed by Mangipudi *et al.* [23], who used the finite element approach to account for the gradual plasticisation of cell walls. They focused the analysis on the combination of material hardening and geometric hardening–due to the reorientation of inclined struts–on the plastic deformation during in-plane tensile loading. The review of literature reveals that analytical studies to calculate the elasto-plastic response and recoil of honeycomb structures is missing. Motivated by this, here we present analytically obtained plastic response, recoil, followed by their parametric dependence. A scaling ansatz and a master-curve, that captures this behaviour, is derived further.

In this work, we ignore the geometric non-linearity due to large deflection of the cell walls. This choice is deliberate as the motivation of the present work is

to study the role of structural and material parameters in the *plastic* response of honeycombs. We do acknowledge, however, that there may be significant geometric non-linearity present in the response of the actual lattice structure–presently excluded from consideration. In a similar manner, shear effects within the cell walls and their stretch deformations have been ignored and the analysis is restricted to the thin cell wall idealisation. These effects could be potentially included in the analysis (e.g. by the use of Timoshenko shear correction factors, or by allowing cell walls to extend along their length)–deemed unnecessary and a distraction to the main motivation of the present work. The validity of these simplifications, in order to facilitate the analysis, has been carried out numerically which gives confidence in our approach.

This paper is organised as follows. An analytical method to calculate the non-linear response due elasto-plastic cell wall bending is formulated in the next section. This accounts for partial plasticity through the thickness, and along the length, of a cell wall. Following this, a method of calculation of spring back upon removal of external in-plane load is presented. Illustrative examples, results and discussions are presented in Section 3. Dependence of response upon the parameters of the honeycomb are systematically studied and the scaling laws thus identified. Concluding remarks are presented in Section 4.

2. Cell wall plasticity and the apparent response of lattices

Consider an infinite two-dimensional cellular sheet, which is loaded remotely by a uniaxial stress (σ_∞) as shown in figure 1 (a). While the state of stress in any real structure is three dimensional, it is reasonable to treat the problem as one of plane stress when the dimension in the depth direction b is significantly smaller than the typical dimensions within the plane. Further, for thin cell walls, one-dimensional models are adequate. The constituent cell wall material is assumed to be elastic-perfectly plastic, thus no hardening occurs beyond yield; the stress-strain relationship is idealised in figure 1 (b). Here E is the Young's modulus and σ_y the yield stress of the cell wall material. The geomet-

ric parameters of the honeycomb are defined in figure 1 (c). In many practical honeycombs, the thickness of the vertically aligned cell walls is $2t$ which results from manufacturing considerations, as such honeycombs are often fabricated by bonding several sheets of the material together with periodically placed gaps and pulling them apart to form honeycombs. However, we restrict our attention to honeycombs of equal cell wall thickness t, as also considered by Gibson and Ashby [24].

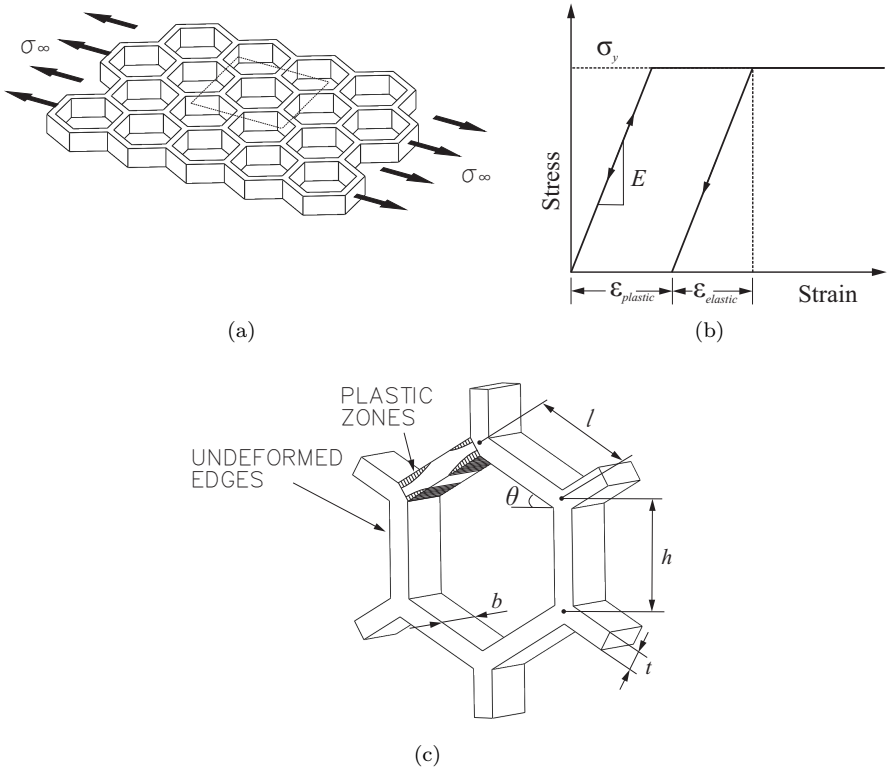

Figure 1: (a) An infinite honeycomb sheet, loaded remotely as shown, (b) Stress-strain relationship that describes the material behaviour of the cell walls (c) geometric parameters associated with a typical hexagonal cell.

When a honeycomb is loaded with a uniaxial remote stress, the cell walls bend and stretch. A typical inclined cell wall before deformation is shown us-

ing the straight line AB in figure 2 (a). The stretch part is ignored here; the deformed shape taken by the cell wall is shown in figure 2 (a) using the curve AB'. This can be justified on the grounds that the topology of the lattice is kinematically mobile leading to a bending dominated behaviour [25]. Significant stretch will be present for $\theta \to 0°$; we have ignored such extreme cases. Results are presented for $\theta > 15°$ for which, in the following sections, we obtain analytical results based on this simplification. They agree well with computations which include stretch–thus justifying the approach. The so-called $P - \delta$ effect is also neglected as its exclusion does not affect the results in the subsequent sections–this is confirmed by comparing analytical results against numerical computations.

The free body diagram of a typical inclined cell wall is shown in figure 2 (b). The remote stress σ_∞, parallel to the x-direction (horizontal), is applied to an infinite honeycomb sheet. Mirror symmetry about the vertical cell walls, combined with equilibrium, dictates that the force along the y-direction F_y is equal to zero. The force along the x-direction F_x and the moment M at location ξ along the length are respectively given by [1]

$$F_x = \sigma_\infty (h + l \sin\theta) b \quad \text{and} \quad M = F_x \sin\theta l(\xi - 1/2). \tag{1}$$

Here, b is the depth of cell walls perpendicular to the plane of the honeycomb and $0 \leq \xi \leq 1$, $\xi = x/l$, is the non-dimensional coordinate along the cell wall.

Plasticity introduces nonlinearity in the response. While many engineering problems require analysis to ensure stresses below the plastic limit, in applications such as the deployment of biomedical stents, or crash during impact, a detailed knowledge of the energy absorbed during the plastic phase of deformation is required. Further, there is no practical interest in response beyond collapse–the point when the cross-section of a cell wall becomes fully plastic. In case of tubular lattice structures such as stents, this corresponds to the collapse pressure: again beyond which there is no practical interest. Hence the analysis presented here is restricted to point when the collapse mechanisms are formed.

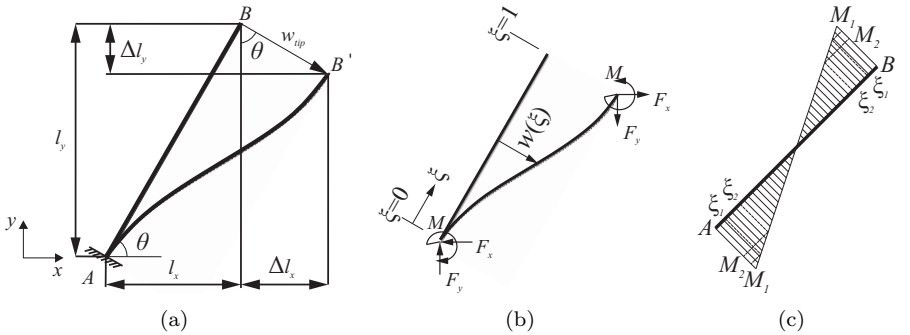

Figure 2: (a) Cell wall bending under remote horizontal stress applied in the x-direction. A typical undeformed cell wall is denoted by the inclined straight line AB. The deformed state of the same cell wall is shown by the curve $AB\prime$ when plotted in a coordinate system attached to the root; (b) Free body diagram of an inclined cell wall under remote stress; (c) Bending moment distribution along a cell wall AB.

The usual assumptions of thin beam theory are accepted here. Firstly, plane cross-sections are assumed to remain plane upon bending. Secondly, the length of the cell wall l is much greater than the cross-section dimensions; therefore, strain energy due to shear stresses can be ignored. This is commonly accepted for the flexural response of thin structures even when shear stress may not be insignificant, because it is the relative importance of the energy terms that determines what deformations could be excluded from consideration. The present approach makes use of the stress distribution across each cross section to calculate the curvature, which is then related to the deflection. The symmetry of the geometry dictates that the deformed cell walls have a point of inflection at their length-wise centre. Being an inflection point implies that $\partial^2 w/\partial \xi^2 = 0$ and, therefore, the absence of bending moment at the relevant cross-section. Here $w(\xi)$ is the deflection of the cell wall at ξ transverse to the cell wall orientation. Thus half of the cell wall reduces to a problem of elasto-plastic bending of a cantilever beam with tip loading which has both axial and transverse force components, but is moment-free. Again, the symmetry ensures that the cell wall joints do not rotate during the application of the remote stress.

Cantilever beams under plastic deformation and spring back have been previously studied by Yu and Johnson [26] in the context of forming of sheet metal

parts. The calculation of the load-curvature relationship for a cantilever beam subjected to a tip load at arbitrary inclination, can now be adapted to obtain the response of lattice structures subjected to remote stresses. The bending distribution moment along the cell walls due to remote loading needs to be calculated first. The cell walls are subjected to a concentrated force and a flexural moment at the two ends, as shown in figure 2 (b). The bending moment distribution along a cell wall AB caused by the applied loads is shown in figure 2 (c).

The maximum bending moment along the length of the cell wall appears at the two extremes and is given by

$$M^* = F_x \sin\theta(l/2) = \sigma_\infty bl \sin\theta(h + l\sin\theta)/2. \tag{2}$$

The shape of the plastic zone within the cell walls can now be analytically calculated, once we realise that there are three qualitatively different distributions over a cross-section possible (see e.g. Johnson [26]). The extent of plasticity depends upon the combinations of M, the bending moment at any cross-section along the cell wall, and N, the axial force. Figure 3 shows the three possible distributions of the elastic/plastic regions through the thickness of a cell wall: (1) completely elastic stress distribution, (2) primary plastic stress distribution: here yield occurs only on one side of the beam (PI), and (3) secondary plastic stress distribution: here yield occurs on both sides of the beam (PII).

All the fibres in the cross-section do not plastically deform simultaneously which leads to the formation of plastic zones of non-trivial shape within cell walls. When a cross-section is partially plastic, outer fibres plastically deform but the inner fibres remain elastic. The two plastic regimes can be identified in the cell walls via cross-sections labelled (2) and (3) respectively, as shown in figure 3. Parts of the cell wall remain completely elastic–such a typical section is denoted by (1) in the figure. Note that ξ_1 and ξ_2 represent the boundaries of the primary and secondary plastic regimes along the inclined cell wall. Thus

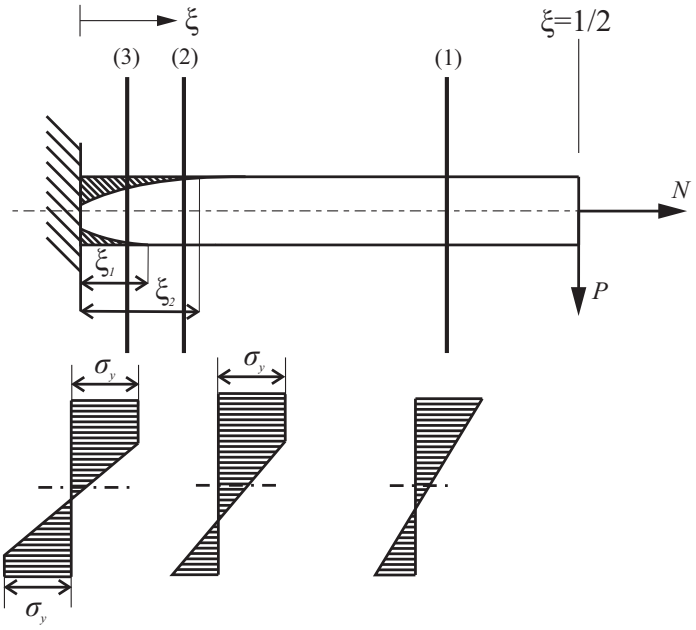

Figure 3: Half of a cell wall modelled as a thin beam simultaneously in flexure and axial tension. The coordinate system is attached to the left end. Note the depth of penetration of plasticity varies along the length and through the thickness of the cell wall giving rise to the shape of the plastic zone as schematically shown. The through-the-thickness stress distribution is shown at three cross-sections along the length at stations (1), (2) and (3).

$\xi > \xi_2$, $\xi_1 \leq \xi \leq \xi_2$, $0 \leq \xi \leq \xi_1$ are the regions of completely elastic, PI and PII deformations respectively. Since the force F_x is inclined at an angle θ to the horizontal, the shear and the axial components of the force at the end are given by

$$\begin{cases} P = F_x \sin\theta = \sigma_\infty \sin\theta(h + l\sin\theta)b \\ N = F_x \cos\theta = \sigma_\infty \cos\theta(h + l\sin\theta)b. \end{cases} \tag{3}$$

Having established the relationship between the lattice parameters and the remote stress with the forces and moments at the centre of the span of a cell wall, we are now in a position to work out the elastic and plastic response.

Since the centre of a cell wall at $\xi = 1/2$ is a moment-free point, the analysis of [26] becomes applicable. The load-curvature relationship [26]

$$\begin{aligned} \phi &= m && \text{for wholly elastic} \\ \phi &= 4(1-n)/\left(3-\frac{m}{1-n}\right)^2 && \text{for } PI \\ \phi &= 1/\sqrt{3(1-n^2)-2m} && \text{for } PII \end{aligned} \tag{4}$$

can now be used. The dimensionless moment $m = |M|/M_e$, axial force $n = |N|/N_e$ and curvature $\phi = |\kappa|/\kappa_e = \left|\partial^2 w/\partial\xi^2\right|/\kappa_e$ are used in equations (4). $M_e = \sigma_y bh^2/6$, $N_e = \sigma_y bh$, $\kappa_e = 2\sigma_y/(Eh)$ are the reference quantities for moment, axial force and curvature. Expressions for n and m^*, the dimensionless value of m at the root of a cell wall, are given by

$$\begin{aligned} n &= (\sigma_\infty/\sigma_y)\,[1+(l/h)\sin\theta]\cos\theta \\ m^* &= 3(\sigma_\infty/\sigma_y)(l/h)\sin\theta\,[1+(l/h)\sin\theta] \end{aligned} \tag{5}$$

which depend on the remote stress and the geometry of the lattice as well as that of cell walls. The value of the axial force n remains unchanged along the length of a cell wall. Equation (4) represents a set of three second order linear differential equations due to the presence of the term $\phi = \left|\partial^2 w/\partial\xi^2\right|/\kappa_e$, each valid for the three separated regions. In order to calculate the cell wall deflection, the above expressions in equation (4) must be integrated in each region and the boundary conditions at the left end need to be used to solve the differential equations. The stress distribution is asymmetric with respect to the centre of the beam. Therefore, the deflection along the whole beam under elasto-plastic loading can be obtained by integrating equations (4) along half of the beam and then copying the solution onto the remaining half, noting the two-fold rotational symmetry of the deflected shape.

Having considered the mechanics of an individual cell wall, the apparent elasto-plastic response can now be calculated analytically for the complete lattice. Apparent properties are those that describe the behaviour of structural material as if the lattice were filled with homogeneous matter possessing these

properties. Such properties are denoted within angular brackets in subsequent discussions. The change in the overall vertical and horizontal dimensions, when a uniaxial load is applied at infinity, are related to the projections of the tip displacement along the horizontal and vertical directions of cell walls, as shown in figure 2 (a). The horizontal and vertical projections of a cell wall, before the application of remote stress, are l_x and l_y, respectively. The changes in projections of the deformed cell wall upon the application of remote stress are denoted respectively by Δl_x and Δl_y. The stretch deformation is ignored, therefore the length of the cell wall is unchanged. Axial stretch of the cell walls is ignored even though the effect of axial force in shifting the neutral axis is included in our subsequent calculations. Therefore the segment BB' in figure 2 (a)is perpendicular to the undeformed cell wall orientation. As stated in the introductory section, geometric nonlinearity resulting from nonlinear strain displacement relationship in the cell wall bending kinematics is ignored too.

Using the tip deflection expression developed in [26], changes in the projections of an inclined cell wall, along and across the application of the load, can be calculated as

$$\begin{aligned}
\Delta l_x &= \frac{4l^2\sigma_y}{hE}\left\{\frac{1}{6}m^*[2-\xi_2^2(3-\xi_2)] + \left\{\tfrac{m^*}{2}\left[1-\left(\frac{1-n}{m^*}\right)^2\right] + \left(\frac{\mathrm{d}\eta}{\mathrm{d}\xi}\right)_2\right\}(1-\xi_2)+\eta_2\right\}\sin\theta \\
\Delta l_y &= \frac{4l^2\sigma_y}{hE}\left\{\frac{1}{6}m^*[2-\xi_2^2(3-\xi_2)] + \left\{\tfrac{m^*}{2}\left[1-\left(\frac{1-n}{m^*}\right)^2\right] + \left(\frac{\mathrm{d}\eta}{\mathrm{d}\xi}\right)_2\right\}(1-\xi_2)+\eta_2\right\}\cos\theta
\end{aligned} \tag{6}$$

where η_2 and $\left(\frac{\mathrm{d}\eta}{\mathrm{d}\xi}\right)_2$ represent the normalised transverse displacement and rotation of a cell wall at ξ_2, where $\eta = wtE/(2l^2\sigma_y)$ is the non-dimensional transverse displacement. These changes in the projection of the cell wall along and across the loading, given by Δl_x and Δl_y respectively, are implicit functions of the remote stress σ_∞ via expressions (5) for n and m^*.

An expression for the displacement transverse to a cell wall can be found

for each point along the cell wall. Each combination of n and m results in a different cell wall stress distribution. Therefore, a different load-curvature expression from the three cases in equation (4) must be used while integrating the curvature relationships. The change in the overall dimensions of the lattice is completely determined by the tip displacement of the inclined cell wall and the lattice geometry. Thus, the calculation of the tip displacement of an inclined cell wall is the crucial part of the present analysis. The apparent strains in directions parallel and perpendicular to loading as functions of the remote stress σ_∞ and the lattice parameters are given by

$$\epsilon^{\parallel}_{\text{app}} = \sqrt{\Delta l_x^2 + \Delta l_y^2}\tan\theta/l \quad \text{and} \quad \epsilon^{\perp}_{\text{app}} = 2\sqrt{\Delta l_x^2 + \Delta l_y^2}\cos\theta/(2l\sin\theta + h). \tag{7}$$

Here $\sqrt{\Delta l_x^2 + \Delta l_y^2} = w_{\text{tip}}$ is the deflection of the tip of a cell wall with respect to the root. The above is a closed form analytical expression for the functional form $\epsilon^{\parallel}_{\text{app}}(\sigma_\infty)$ and $\epsilon^{\perp}_{\text{app}}(\sigma_\infty)$ which relates remote stress σ_∞ to the components of the apparent strain of the cellular sheet, in the direction of, and lateral to, loading. The remote stress implicitly appears inside the expressions for $\Delta l_x(m^*, n)$ and $\Delta l_y(m^*, n)$ which, in turn, contain the remote stress within the expressions for $m^*(\sigma_\infty)$ and $n(\sigma_\infty)$.

The above development is generic for any lattice having the geometry of a cell described by figure 1 (c). This includes negative angle θ which provides us with the interesting opportunity to examine the elasto-plastic response of lattices with apparent auxetic behaviour in the post-plasticity regime of deformation.

The spring back behaviour of infinite lattices can now be analytically assessed by considering the unloading scenario. The elastic recovery is via a linear path on the stress-strain plane. Since different points within the lattice are at different levels of plasticity, the residual plastic deformation has a spatial distribution within the honeycomb. In order to analytically calculate the spring back of lattice materials, unloading of the bent cell walls must be taken into consideration to determine their final curvature. As previously done for

the loading calculations, the unloaded configuration of the key points on lattice can be calculated by focussing the attention to the tip deflection of a bent cell wall upon elastic recovery. The elastic deflections corresponding to the moment applied at a section must be subtracted from the deflections before unloading. The x- and y-components of the permanent tip deflection of the cell wall with respect to its root are thus given by

$$\begin{aligned} w_x^{\text{permanent}} &= \Delta l_x - \frac{2}{3}\frac{m^* l^2 \sigma_y}{tE}\sin\theta \\ w_y^{\text{permanent}} &= \Delta l_y - \frac{2}{3}\frac{m^* l^2 \sigma_y}{tE}\cos\theta \end{aligned} \tag{8}$$

where the first term in each of the two expressions is given by equation (6). After the removal of the external load, the residual stress distribution over a cross-section must be self-equilibrated.

3. Results and discussions

Analytical results as well as computational verifications for response in the plastic range, spring back and recoil, and lateral response leading to apparent Poisson's contraction for elasto-plasticity are provided in this section. The effect of ignoring stretch deformation, in order to facilitate analysis in the previous section, is also brought out. These results are organised into several subsections with relevant discussions contained there in.

3.1. Non-linear elasto-plastic response of honeycombs

Having developed analytical expressions for the response of a honeycomb sheet beyond yielding–by incorporating elasto-plastic response of thin cell walls into the calculation, we are now in a position to quantitatively present the apparent non-linear response of such structured material. When remote stress is applied, the initial phase of the response will be purely elastic, as the cell walls are under completely recoverable elastic deformation. In this phase, remote stress varies linearly with the apparent strain in the direction of the applied

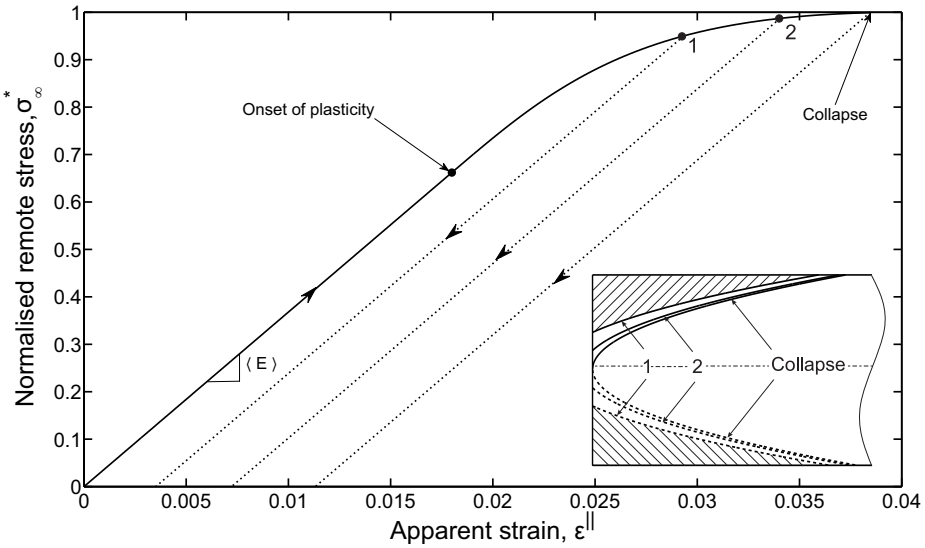

Figure 4: Tensile stress-strain curves for an infinite honeycomb sheet subjected to a remote uniaxial stress along the x-direction. The normalised stress $\sigma^*_\infty = \sigma_\infty/\sigma_{\text{Collapse}}$ is plotted against the apparent strain parallel to the direction of the application of the load. The slope of the apparent stress-strain curve equals the apparent Young's modulus $\langle E\rangle$ of the lattice;the tangent modulus diminishes beyond yielding.

loading–the slope being a measure of the apparent Young's modulus $\langle E\rangle$ of the honeycomb. This behaviour is well documented and thoroughly studied in the past by Gibson *et al.* [1, 24]. The apparent modulus of elasticity was calculated using the implicit but closed form equation (6) for low values of remote stress such that all material points on the honeycomb are within the elastic limit. This requires turning the displacements into apparent strain quantities (equation (7)). The values thus obtained for the apparent modulus match extremely well (up to 4 significant figures) with the well known benchmark results (Gibson and Ashby [24]). This provides a validation for the more general expression developed in this paper up to the point of transition to plasticity. The part of the curve in figure 4 from the origin up to the point labelled 'onset of plasticity' represents this validation.

Consider now an infinite regular lattice shown in figure 1 (a) subjected to a remote in-plane stress along the x-direction such that cell walls yield beyond

the elastic limit. Equation (6) together with equation (7) can be taken as the apparent stress-strain relationship for the honeycomb under plastic deformation. This implicit but analytical relationship requires eliminating Δl_x and Δl_y. The remote stress σ_∞ enters (6) *indirectly* via the terms m (whose maximum value along the cell wall length is m^*) and n according to the expressions in equation (5). The results of these calculations are shown in figure 4, where the stress at infinity has been normalised with respect to the collapse stress $\sigma_\infty/\sigma_{\text{Collapse}} = \sigma^*_\infty$; the collapse stress is the value of the remote stress which corresponds to the cell wall cross-section at the joints becoming fully plastic. The generic feature of this curve is an initially linear elastic phase extending up to the onset of plasticity followed by a nonlinear regime. Note also that the tangent modulus at the onset of plasticity shows continuity, i.e. the apparent stress vs apparent strain curve is smooth at the transition from elasticity to plasticity. This is in contrast with the constitutive law for the parent material which shows discontinuity of tangent modulus at the point of yielding. This is because, while the material stress-strain curve is not differentiable at the point of elastic-to-plastic transition, the strain energy density is continuous with respect to material strain and the evolution of plastic zone is without a jump. This leads smoothness (hence differentiability) of the remote stress with respect to apparent strain for the lattice. In other words, the whole structure does not become plastic simultaneously; so despite discontinuity in the tangent modulus of the parent material, the apparent modulus of the cellular solids is continuous.

Two arbitrary points along the apparent stress-strain curve are marked in figure 4 (labelled '1' and '2'). The corresponding contours of elastic-plastic region boundaries are shown in the inset for a section of the cell wall. The three sets of contour lines labelled '1', '2', and 'Collapse' correspond to the corresponding labelled points on the apparent stress-strain curve. The solid lines in the inset are associated with tensile stress whereas the dotted lines with compressive stress. These lines denote the boundary between the elastic region and the plastic region for different phases of plasticity. All points between these curves and the outermost fibres are plastic. Curves above and below the neutral

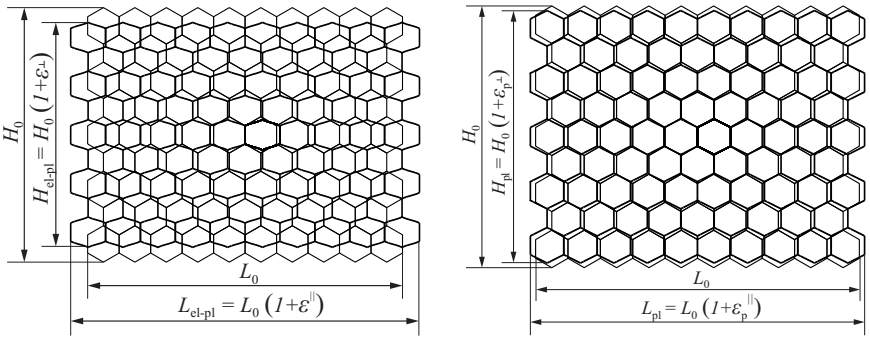

Figure 5: (a) Elasto-plastic deformation of an infinite honeycomb sheet subjected to a remote tensile stress along the x direction. (b) Spring back of the same sheet as in (a)–note that the horizontal shrinkage is accompanied by a lateral extension during spring back.

axis show a minor asymmetry which is apparent on closer inspection–the reason for asymmetry being the presence of axial loading on the compressive side and the tensile side of flexural response, thus changing the stress distribution over the cross-section that lacks symmetry with respect to loading. The deformed shape of the lattice as calculated for the non-linear plastic regime is shown in figure 5 (a).

When the remote stress is further increased, the apparent tangent modulus continues to decrease until the cross-section at the root of a cell wall becomes completely plastic. The total moment at this cross-section equals that corresponding to a plastic hinge. We would refer to this remote stress as the collapse stress because the lattice is unable to resist any greater remote stress. The remote stress corresponding to collapse was given by Gibson and Ashby [1] and the values obtained here confirm this. However, the non-linear curve bridging the linear part of the response to the point of collapse has not been reported before. The present work fills the gap between the previously known elastic limit and the completely plastic extreme via new results in the non-linear response range as well as recoil. This is further characterised qualitatively and quantitatively in the subsequent sections.

3.2. Unloading and recoil

Consider now the unloading problem from the post-plasticity phase. Frequently one needs to quantitatively assess the permanent strain and deformation after a piece of lattice material has undergone plastic deformation. For example, for repetitive structures such as cardiovascular stents, there is a need to know the recoil of the structure post-plastic phase in order to know the shape of the medical device after its deployment. Radial recoil is a key-performance parameter during stent deployment which can be related to the recoil of flat lattice structures. Since we are concerned only with the generic hexagonal lattices in the present paper, we will not make these connections here. Plasticity calculations are also critical for calculations involving crash and impact. In all these practical situations, previously known linear elastic response calculations are not adequate–this highlights the motivation and enhances the value of the the present work.

The apparent stress-strain curve of the lattice is dependent on the unloading path on the material law of the parent material as well as the lattice geometry. Assuming the strain recovery to be linear and parallel to the loading path on the material curve, the residual apparent plastic strain and spring back of the lattice are calculated here. They are shown using dotted lines with an arrow in figure 4. The return shows a path parallel to the apparent modulus of elasticity during elastic loading. This is expected because the recovery has been assumed to follow a linear stress-strain law with the modulus of elasticity the same as that of a the parent material in the cell walls. Consider that the remote stress is now removed. The deformation related to the elastic part is recovered; therefore only the permanent plastic deformation remains within the structure. The final shape after the spring back is shown in figure 5 (b).

In order to quantify the spring back of a lattice, it is useful to define the percentage recoil R for a lattice as

$$R = \left(\frac{L_{\mathrm{el-pl}} - L_{\mathrm{pl}}}{L_{\mathrm{el-pl}} - L_0} \right) \times 100. \tag{9}$$

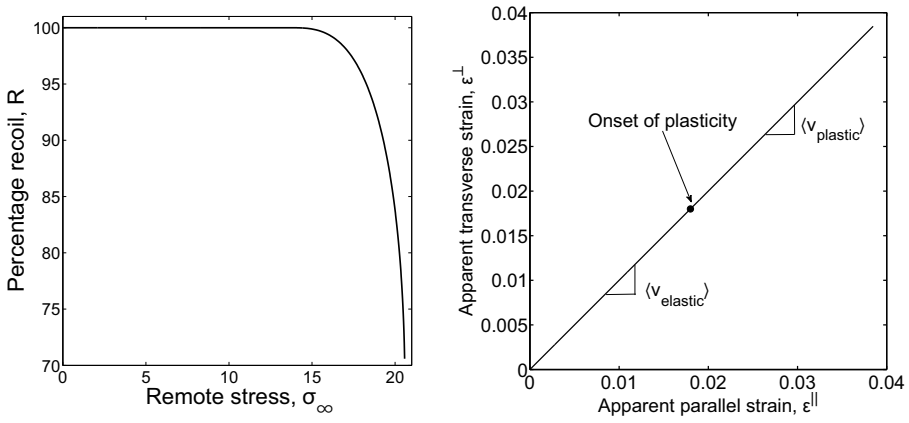

(a) (b)

Figure 6: (a) Percentage recoil for a honeycomb sheet loaded remotely along the x-direction. (b) The dependence of the apparent lateral strain $\epsilon^{\perp}$ on the apparent longitudinal strain $\epsilon^{||}$. The slope that represents the apparent Poisson's ratio $\langle\nu\rangle$ of honeycomb is same and constant in elastic and plastic regimes.

Here L_0 is the initial length of the sheet, $L_{\mathrm{el-pl}}$ the length of the hexagonal sheet when loaded at infinity and L_{pl} its length upon removal of the load, thus only plastic deformation remains within the structure. Having taken a unit cell approach, the expression for R obtained here is valid for an infinite lattice. This parameter has been plotted in figure 6 (a). Recoil is observed along as well as across the loading-unloading directions. Lateral response and recoil are discussed next.

3.3. Apparent Poisson-contraction

The horizontal and vertical responses, as well as percentage recoil, are found to be equal for a regular hexagonal lattice. This is a manifestation of the fact that the apparent Poisson's ratio equals 1 for regular hexagonal honeycombs. The apparent stress-strain curve along the direction perpendicular to the application of the load is not shown here as it shows a behaviour very similar to figure 4, except that the strain is negative indicating that the structure *shrinks* laterally.

The apparent Poisson's ratio is defined as the negative of the ratio of the

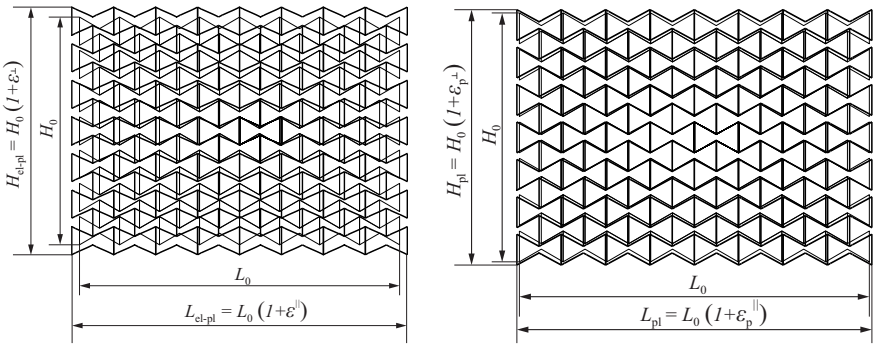

(a) (b)

Figure 7: (a) Deformation of an auxetic lattice structure through plastic phase when tensile loading is applied in the horizontal direction. Note the accompanying lateral expansion. (b) Spring back upon release of load showing longitudinal as well as lateral contraction.

lateral strain to the the applied strain

$$\langle \nu \rangle = -\frac{\epsilon^{\perp}}{\epsilon^{\parallel}} = -\frac{\Delta l_y}{l_y}\frac{l_x}{\Delta l_x}, \tag{10}$$

where the changes in the projection of the inclined cell wall Δl_x and Δl_y in the x- and y-directions are respectively given by

$$\Delta l_y = w_{\text{tip}} \cos\theta \quad \text{and} \quad \Delta l_x = w_{\text{tip}} \sin\theta, \tag{11}$$

where w_{tip} is the deflection of an inclined cell wall relative to its root transverse to the inclination of the cell wall (figure 2 *a*)–the common leading terms between the two expressions in equation (6). Gibson *et al.* showed (see [1]) that the apparent Poisson's ratio $\langle \nu \rangle$ during linear elastic response equals 1 for regular hexagonal honeycombs. Under elastic deformation, the apparent Poisson's ratio is completely independent of the constituent material properties for thin walled cellular solids as argued by Bhaskar [27]. It is not obvious as to how the apparent Poisson's ratio $\langle \nu \rangle$ would change in the non-linear regime of deformation.

Dimensional and scaling arguments, in situations where exact answers are difficult to obtain, are often very effective [28, 29]. Following the approach

in [27], the tip deflection of a cell wall with respect to its root w_{tip} has the functional form

$$w_{\text{tip}} = f(\text{geometry}, E, \nu), \tag{12}$$

while the lengths along the x- and the y-direction are dependent on the lattice geometry, i.e.

$$l_x = f(\text{geometry}) \quad , \quad l_y = f(\text{geometry}). \tag{13}$$

From equations (10) and (11), it is apparent that the tip displacement w_{tip}, which depends on the material properties, is cancelled out from the expression of $\langle\nu\rangle$. Therefore the apparent Poisson's ratio becomes a function entirely of geometric parameters l_x, l_y, $\sin\theta$ and $\cos\theta$. Thus the dimensional argument combined with the kinematics and mechanics of cell wall deformation dictate the apparent Poisson's ratio should be the same as that for the elastic limit lattice response, which is known to be equal to 1. This is confirmed by the detailed calculations as shown in figure 6 (b) which shows the dependence of the transverse strain as a function of the longitudinal strain–the slope of this curve being unity for the entire range of elasto-plasticity.

3.4. Plastic response and spring back of auxetic *lattices*

Most real materials exhibit positive Poisson's ratio as the material shrinks in the direction lateral to the that of loading. However, there has been recent interest in structured material that show apparent negative Poisson's ratio. Such material, when loaded in one direction, respond by expanding in the lateral direction and are known as *auxetic* [30, 31]. Simple models of auxetic planar material can be constructed by rendering the hexagons to be non-convex. This is easily achieved by allowing the angle θ in figure 1 (c) to be negative. When such a structure is subjected to tensile remote stress, it will simultaneously extend along, and lateral to, the direction of loading. Elastic response of such

auxetic material can be predicted using the theory previously presented by Gibson and Ashby [1]. Here we present the *elasto-plastic response* of such auxetic lattice in figure 7 (a). The apparent stress-strain curve can now be calculated analytically (not shown for sake of brevity); it has trends similar to those of non-auxetic lattices–there is a proportional regime of completely recoverable elasticity followed by a softening part that is continuous and differentiable, despite the constitutive relationship for the parent material of the cell walls being piece-wise linear. Upon release of the remote stress, the spring back also shows auxetic behaviour in that the lattice shrinks in *both* directions simultaneously (see figure 7 b).

When auxetic honeycombs are stretched or compressed in a given direction, the apparent lateral strain is tensile or compressive respectively. This does not mean that the cell walls would be in significant axial compression. Hence buckling of cell walls is not considered as bending continues to be the only dominant mechanism of cell walls deformation. This would not be the case, however, if the material is laterally constrained forcing cell wall buckling. Lateral constraint can lead to cell wall buckling even for non-auxetic architectures. Such situations are kept out of consideration here.

3.5. The effect of cell wall stretch and geometric non-linearity

The model of cell wall plasticity developed here ignores stretch. It proves to be technically cumbersome to include the stretch deformation when the deformation is plastic because of the invalidity of the superposition principle for non-linear response. However, the effect can be easily assessed computationally and this is presented in figure 8. The solid line represents the analytically calculated plastic response of a lattice for the elastic-perfectly plastic material model ignoring stretch and geometric non-linearity. The dashed line in the figure represents computational results based on a unit cell (as shown in the inset; note that hexagon is not a unit cell). The agreement between the analytical results presented here and the computational results which make use of finite elements is excellent for the whole range of elasto-plastic response up to the point of col-

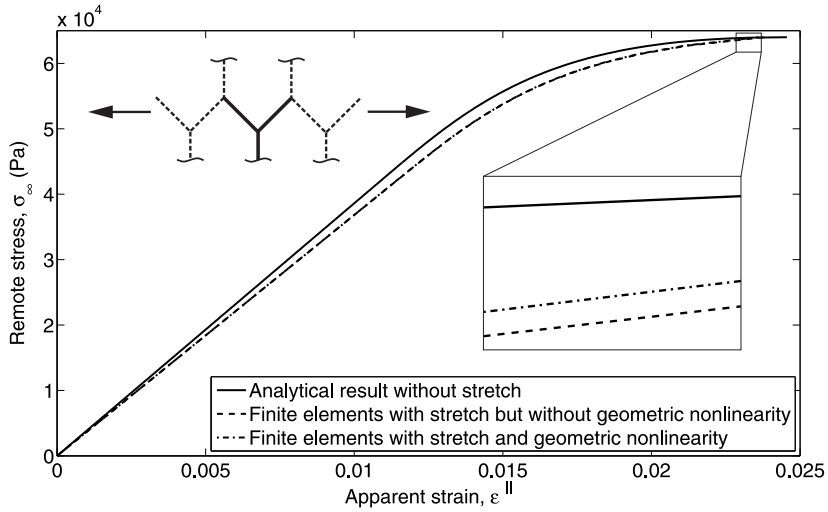

Figure 8: Remote stress as a function of the apparent lattice strain. The solid line refers to the analytical results which ignore the stretch and the geometric nonlinearity. The effect of stretch (dashed line) and the geometric nonlinearity (chain line) are negligible for thin cell walls.

lapse. The unit cell has been modelled as a 3D structure using the element type C3D8I (8-node brick element,) within the commercial code ABAQUS. This element has geometric as well as material non-linearity capability which could be switched on or off at will. The number of degrees-of-freedom per node is 3 and the total number of elements over 25,000 which was arrived systematically by increasing this till convergence was achieved well within 1%. The geometric parameters of the lattice are $h = l = 1$ mm, $b = t = 0.02$ mm, $\theta = 30°$. The material parameters are $E = 209$ GPa and $\sigma_y = 240$ MPa. It is interesting to note that the absence of stretch in the model overestimates the apparent stress required for the specified value of apparent strain up to the collapse.

Consider next the role of geometric non-linearity as it may be argued that it could have impact on the response of lattice structures loaded remotely. An overall stiffening of the structure due to geometric non-linearity is observed in the inset of figure 8 as the curve corresponding to the inclusion of geometric non-linearity *in addition to* stretch is slightly higher than that when only stretch is considered (the chain line). These calculations are carried out on a unit cell.

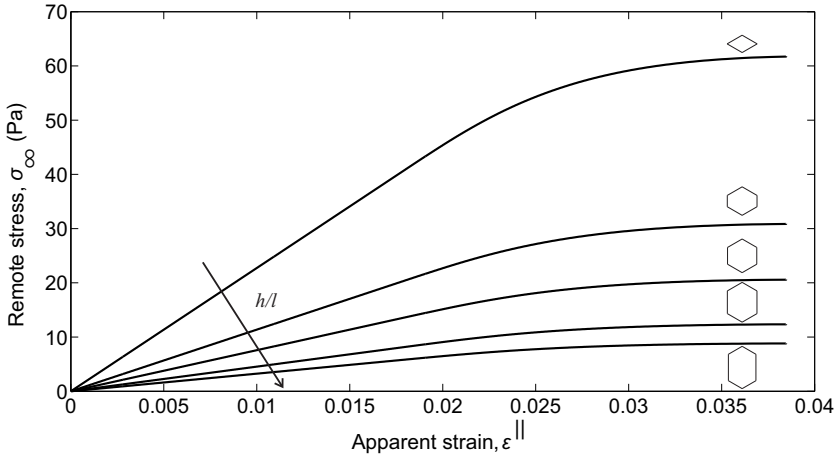

Figure 9: The effect of h/l ratio on the elastoplastic response of hexagonal lattices.

For the lattice parameters considered here (cell wall length to thickness ratio approximately equal to 25), stretch appears to have a greater influence on the response than the geometric non-linearity.

Note that some experimental data is available in the literature, as cited in the introductory section. However, these studies are unsuitable for direct comparison with the results obtained in our work because the scenario in the cited experimental works is rather complex involving compressive crushing, buckling and self-contact of cell walls, which are ignored in the analysis presented here. Here we restrict ourselves to providing benchmark results for remotely stretched honeycombs under plastic deformation–no experimental result for such an idealised situation exits in the literature. Having briefly considered higher order effects and their role in lattice elasto-plastic response, we now return to the main purpose of the paper which is to study in detail the plasticity of such structured material.

4. Scaling arguments and collapse of response curves

The analytical approach developed here affords results for lattice structure in a closed form. A reward of such an analysis is not only to have a benchmark

result (under the assumptions of the model), but also the ability to infer trends of the behaviour and their dependence on the parameters of the problem–as opposed to computations and laboratory experimentation that obscure this insight. On the other hand, both computational and physical experiments are extremely useful in suggesting the dominant features of the behaviour, in addition to guiding the analysis, in order to retain the most significant aspects of a problem within a model. We carry out numerical calculations in this spirit first, and then propose a scaling ansatz which unifies results for a family of problems for the bending dominated lattice response under plastic deformation.

4.1. The dependence of plastic behaviour on lattice parameters

The influence of the ratio of the height h and the length of the cell wall l is now studied while keeping all other material and geometric parameters held constant. By increasing the h/l ratio in steps of $h/l = 0, 0.5, 1, 2, 3$, while other material and geometric parameters of the lattice are held constant at $t/l = 0.012$, $\theta = 30^o$, $E = 209$ GPa, $\sigma_y = 240$ MPa, we observe that the stiffness of the lattice structure decreases, which is evident from figure 9. This provides us with design guideline for energy absorption applications that straight members should be minimised for greater energy dissipation. By contrast, the plastic deformation of rhomboidal cells occurs at a higher load, therefore in order to obtain the same amount of deformation as for honeycomb with longer straight vertical members, a higher load is required. Thus higher energy absorption comes with a price: the stiffness of the lattice becomes greater which is undesirable from the point of view of dynamic energy absorption because this leads to higher dynamic peak forces during impact. The trade-off between peak loads and the plastic energy absorption, that one frequently encounters in many crashworthiness application, is evident here too.

The effect of h/l ratio on the lateral response is shown in figure 10. Clearly, the apparent lattice properties are no longer isotropic. In the linear elastic range of deformation, the apparent Poisson's ratio and the apparent Young's modulus both scale similarly with (h/l) according to $(\langle\nu\rangle, \langle E\rangle) \sim (hl^{-1} + \sin\theta)^{-1}$. Thus,

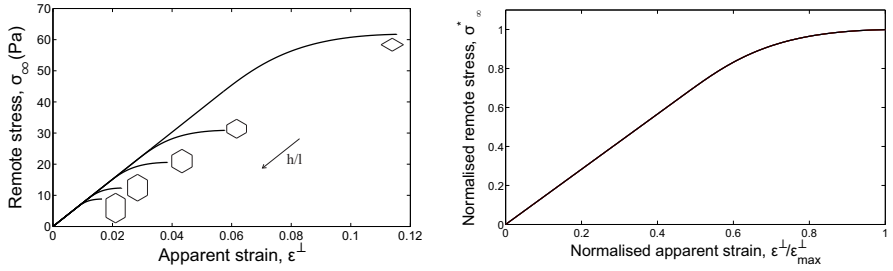

(a) (b)

Figure 10: (a) Plot of the remote stress σ_∞ against the lateral strain $\epsilon^\perp$ for increasing values of the non-dimensional ratio h/l. (b) The curves have been scaled with respect to their collapse stress and maximum strain–all the curve in (a) collapse to a single master curve in (b).

the ratio $\sigma_\infty/\epsilon^\perp$ becomes independent of h/l leading to a common slope for all the curves in the linear range in figure 10 (a). However, in the plastic regime, this is not valid. Cell wall yielding takes place at a lower level of apparent remote stress because lower remote stress correspond to similar cell wall stress for greater h/l. This behaviour is observed from the numerical calculations and is presented in figure 10 (a). The shape of the curves in figure 10 (a) appear to be similar. This is confirmed upon scaling the variables with respect to the maximum values of the lateral strain and the remote stress for each curve. The results are presented in 10 (b) which shows collapse of all the data to a single curve.

The role of thickness to length ratio of a cell wall t/l is investigated next. The ratio $h/l = 1$ is held constant, $\theta = 30°$, $E = 209$ GPa, $\sigma_y = 240$ MPa. The thickness to cell wall length ratio is now varied as $t/l = 0.0088, 0.0120, 0.0177, 0.0243$. For linear elasticity, it is well known that the apparent modulus scales according to $\langle E \rangle \sim (t/l)^3$. When nonlinearity due to plasticity is present then this becomes non-trivial except for the collapse calculation where remote stress corresponding to collapse scales as per $\sigma_{\text{Collapse}} \sim (t/l)^2$. For the non-linear elasto-plastic phase the behaviour appears to be complex and the parametric dependence showing the effect of (t/l) on the apparent response is shown in figure 11 (a). The family of curves are drawn up to the point of collapse. As for the case

of (h/l) ratio, the shape of the curves appears to be similar. Normalising the variables with respect to the values at collapse for each curve results in nearly identical curves–when superposed (see figure 11 b) the slight difference being attributed to the stretch deformation in cell walls.

The nearly overlapping curves in figure 11 (b) suggest the existence of something deeper that may enable us to collapse all apparent stress-apparent strain curves onto a single non-linear function. Given that the elastic part of the deformation is due to the flexure of cell walls and the plasticity is manifested in a complex plastic zone pattern through the thickness of each cell wall, we seek renormalisation of the loading and response variables in the hope that dimensional groups may appear as appropriate scaling parameters that would achieve this data collapse. A promising direction would be to seek such a universal non-linear response curve for a single cell wall first, which could later be related to lattice response via honeycomb geometry. This is taken up next.

4.2. Separation of lattice geometry from cell wall properties, scaling arguments and data collapse

Having considered hexagonal lattices for a lattice geometries that differ in their lattice parameters such as l, h, and θ, we are now in a position to separate the cell wall mechanics from the kinematics of the lattice deformation. The similarity in the shapes of the parametric trends of the apparent stress vs apparent strain of the elasto-plastic response of such structured material, as observed previously, suggests the existence of scaling of variables and an appropriate renormalisation. For the linear response of bending dominated cellular solids, the scaling of the apparent modulus of elasticity, as per $\langle E \rangle \sim E(t/l)^3$, is not enough to collapse the non-linear deformation profiles to a single curve. The process of identifying *new stretch variables* for the apparent strain and the apparent stress is non-trivial. Because of a greater number of variables (e.g. the yield stress σ_y) now, further arguments beyond dimensional homogeneity are required. These could include physical reasoning and approximations. There is no guarantee that one would be able to be successful to obtain such renor-

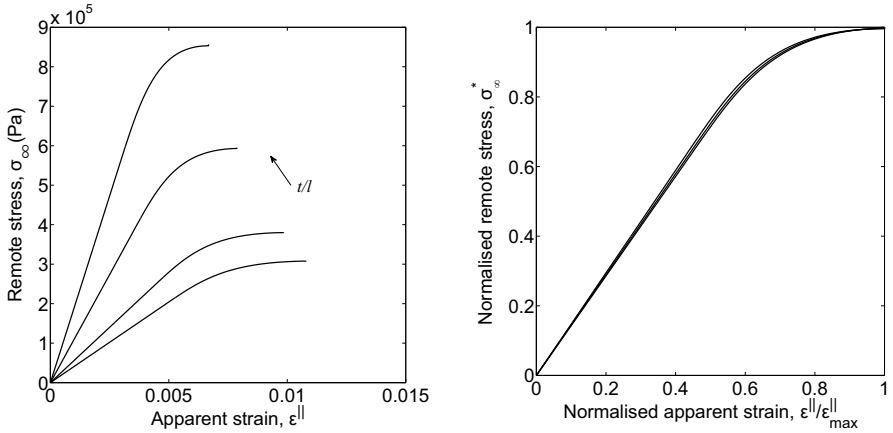

(a) (b)

Figure 11: (a) Effects of the ratio between cell wall thickness t and strut length l on the mechanical response of the lattice structure. (b) The curves have been scaled with respect to their collapse stress and maximum strain they approximately overlap onto each other.

malisation: when this is possible, it is practically useful, theoretically unifying and insightful. We will discover later in this section the appearance of terms involving σ_y, t, l on scale factors for the apparent stress as well as apparent strain relating *a complex non-linear relationship*.

To develop scaling variables that collapse the non-linear response curves onto a single master curve, consider a cantilever beam with transverse tip force P, axial force N, length L, thickness t and depth in the direction perpendicular to the plane of deformations b (see inset in figure 12). The elastic-perfectly plastic constitutive relationship is described by *two material parameters*: the Young's modulus E and the yield stress σ_y. The tip deflection for this beam flexure problem is given by δ. The scaling arguments for linear elasticity of cellular solids with beam-like cell walls is straightforward and has been previously presented by Gibson and Ashby [1] and Warner *et al.* [32]. Here we develop scaling relationships further for elasto-plasticity.

Consider the functional relationship $\delta = \delta(P, N, E, \sigma_y, L, t, b)$, for a regular hexagonal honeycomb so that $h = l$, which is an 8-variable problem while applying Buckingham's π-theorem. The reduction in variables is by just two

here (since the variables that do not form a π-group themselves are length and mass$\times$ length^{-2} which occurs in exactly the same form 4 times: in P, N, E, σ_y and must be counted just once). Therefore, the above functional relationship takes the following non-dimensional form

$$(\delta/L) = f_1\left((P/(EL^2)), (N/(EL^2)), (\sigma_y/E), (t/L), (b/L)\right). \tag{14}$$

Dimensional homogeneity cannot take us any further. We need simplifications, assumptions, and further physics in order to discover scaling laws–we will make use of them, in turn, now. (i) The assumption of bending dominance of the lattice architecture leads to δ/L becoming a weak function of $(N/(EL^2))$, i.e. $(\delta/L) = f_2\left((P/(EL^2)), (\sigma_y/E), (t/L), (b/L)\right)$. (ii) The scenario in the depth direction is identical in all the planes (i.e. the displacement field is independent of the depth direction for beam mechanics), therefore (P/b) determines the deflected shape completely. This requirement is satisfied by combining the first and the last non-dimensional terms such that P/b appears together as a single π-number. This results in $(\delta/L) = f_3\left((P/(bLE)), (\sigma_y/E), (t/L)\right)$.

We still need further information to find t/L scaling. This is afforded by the beam curvature-bending-moment relationship

$$\kappa = \frac{\partial^2 w}{\partial x^2} \sim \frac{\sigma_y}{Et}\left[1 - \frac{Px}{bt^2\sigma_y}\right]^{-1/2} \tag{15}$$

where x is the local coordinate measured from the loaded end. Since curvature $\kappa \sim \delta/L^2$ and the term inside the brackets on the right side $\sim PL/(bt^2\sigma_y)$, it suggests the following scaling ansatz

$$\frac{\delta}{\sigma_y L^2/(Et)} = F\left(\frac{P}{\sigma_y bt^2/L}\right), \tag{16}$$

where the unknown non-linear functionality F is yet to be determined. The nature of this unknown function must be such that it is linear up to the point of onset of plasticity.

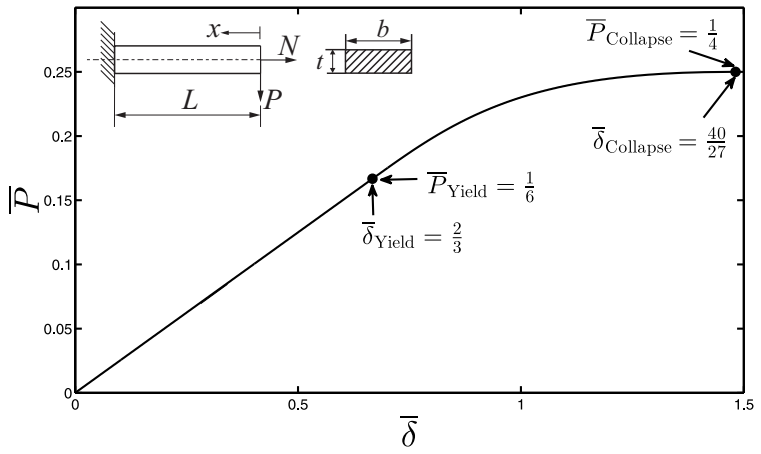

Figure 12: Plot of the non-dimensional force $\overline{P}$ against the transverse deflection $\overline{\delta}$ of a cantilever beam subjected to transverse tip loads P and N. With a suitable scaling of variables *all* the $\overline{P}$-$\overline{\delta}$ relationships collapse to a single master curve–thus providing us with the unknown functionality F. The point $(\overline{P}_{\text{Yield}}, \overline{\delta}_{\text{Yield}})$ corresponds to the onset of plasticity, whilst $(\overline{P}_{\text{Collapse}}, \overline{\delta}_{\text{Collapse}})$ to the collapse of the beam when the cross-section at the root is fully plastic.

Clearly, in linear elasticity, $\delta \sim P$ and $\delta \sim (bt^3)^{-1}$, the tip force for yielding scales according to $P_{\text{Yield}} \sim \sigma_y bt^2/L$, and the tip force for plastic collapse scales as $P_{\text{Collapse}} \sim \sigma_y bt^2/L$. So we could have alternatively sought a scaling ansatz of the form

$$\frac{(\delta/L)}{(\sigma_y/E)} = \left(\frac{t}{L}\right)^{\alpha} f\left(\frac{P}{\sigma_y bt^2/L}\right). \tag{17}$$

Since, the above has to be valid for the linear elastic part of the curve dimensional homogeneity results in $\alpha = -1$, whence we arrive at the sought scaling law (16).

Thus we renormalise the variables according to $\overline{\delta} = \delta/(\sigma_y L^2/(Et))$ and $\overline{P} = P/(\sigma_y bt^2/L)$ so that we get a 'master-curve' describing the non-linear elasto-plastic behaviour of beams subjected to tip loads. This proposed master-curve now includes *all* geometric and material parameters relevant to the mechanics of such a cantilever beam and is presented in figure 12. All the curves for various geometric and material data collapse to this line. This functionality can be

conveniently expressed via the inverse relationship of (3.8) as

$$\overline{P} = G(\overline{\delta}); \tag{18}$$

as it was convenient to treat the elastic response δ as the dependent variable whereas the force at the tip P as the independent variable to develop the relationship (3.8), but the curve in figure (12) and the stress-strain curve are frequently presented with the response variables (defection or strain, respectively) as the independent variable.

Consider salient points on the non-linear functional relationship between the applied force and the tip deflection. Smooth transition to plasticity is observed in the functional relationship $\overline{P}(\overline{\delta})$. We will denote this relationship via a generic function $G(x)$.

The non-linear part of the sought functionality $G(x)$ in equation (16) is analytically tractable and is implicitly available via the relationships such as equation (6) which could be specialised for zero axial force, as shown in figure 12. Two critical points on the curve (i) transition to plasticity when the first outer fibre of a cell wall yields and (ii) plastic collapse when a cross-section becomes wholly plastic can be analytically derived with relative ease. At the onset of yielding, one obtains

$$\overline{P}_{\text{Yield}} = \frac{1}{6}, \quad \text{and} \quad \overline{\delta}_{\text{Yield}} = \frac{2}{3} \tag{19}$$

as the non-dimensional force and the deflections at the onset of plasticity. The corresponding value for collapse are calculated for the completely plastic state of the cell wall cross-section as

$$\overline{P}_{\text{Collapse}} = \frac{1}{4}, \quad \text{and} \quad \overline{\delta}_{\text{Collapse}} = \frac{40}{27} \tag{20}$$

which highlights that the collapse force is 50% higher than the force at which yielding takes place. This value of the tip response of the cantilever beam is obtained from the analytical expression for beam elasto-plasticity discussed in

Section 2 when the axial force is set to zero.

Following a successful scaling analysis of tip deflection in non-linear elasto-plastic deflection of a cell wall, we can infer the apparent elasto-plastic response of infinite lattices subject to remotely applied stress. The apparent strain of lattices scale as $\langle\epsilon\rangle \sim \delta/L$, the apparent stress scales as $\sigma_\infty \sim P/(bL)$. This suggests the functional relationship of the form $\langle\epsilon\rangle/\langle\epsilon\rangle_{\text{ref}} \propto F(\sigma_\infty/\sigma_{\infty_{\text{ref}}})$ where the reference values for the apparent strain and the remote stress need to be established. The proportionality constant would depend on the lattice geometry alone (i.e the length, angle etc. associated with cell walls, but not thickness or material properties). For a lattice of characteristic cell wall length l, we have $l \sim L$. Therefore, the functional form of the remote stress vs apparent strain curve must be similar to that of the $\overline{P} - \overline{\delta}$ curve up to a yet to be determine scaling of the two stress and strain variables. This can be mathematically expressed as

$$\beta\overline{\sigma}_\infty = G\left(\alpha\langle\overline{\epsilon}\rangle\right) \tag{21}$$

where scale factors α and β are still to be determined. Here, the scaled remote stress $\overline{\sigma}_\infty$ and the scaled apparent strain $\langle\overline{\epsilon}\rangle$ are defined as

$$\overline{\sigma}_\infty = \frac{\sigma_\infty}{\sigma_y t^2/l^2}, \quad \text{and} \quad \langle\overline{\epsilon}\rangle = \frac{\langle\epsilon\rangle}{\sigma_y l/(Et)}, \tag{22}$$

respectively. Note the presence of the terms σ_y, t, l within the scaling parameters of *both* remote stress σ_∞ and the apparent strain $\langle\epsilon\rangle$ that are related non-linearly via the function G. With the help of the scaling suggested by equation (3.7), and hence equation (3.8), this has been possible. Previously known scaling such as apparent modulus $\sim E(t/l)^3$, is unable to provide the stretch variables obtained here. Further, for the linear part of G, terms cancel out in a way that the known apparent modulus scaling of $\langle E\rangle$ with t/l and E reappears naturally.

Given the limits of the $\overline{P} - \overline{\delta}$ curve, we conclude that $0 \leq \alpha\langle\overline{\epsilon}\rangle \leq 40/27$ and $0 \leq \beta\overline{\sigma}_\infty \leq 1/4$. Similarity between the $\overline{P} - \overline{\delta}$ and the $\overline{\sigma}_\infty - \langle\overline{\epsilon}\rangle$ curves suggests that there must be correspondence between *physically corresponding* point on

the two curves. One such point is that of onset of yielding, characterised on the $\overline{P} - \overline{\delta}$ curve by equation (3.11). Therefore, we must have

$$\alpha \langle \overline{\epsilon} \rangle_{\text{Yield}} = 2/3, \quad \text{and} \quad \beta \left(\overline{\sigma}_{\infty} \right)_{\text{Yield}} = 1/6. \tag{23}$$

We are now able to develop analytical functional relationship which would make used of the functionality of the master curve $G(x)$ for lattices. To illustrate this for the regular hexagonal lattices, consider the maximum bending moment in the cell walls due to remote stress σ_{∞} as $M = 3\sigma_{\infty} b l^2/8$. Equating this to the fully plastic moment $\sigma_y b t^2/6$, we obtain $\left(\overline{\sigma}_{\infty} \right)_{\text{Yield}} = 4/9$. Substituting this into (23), we obtain $\beta = 3/8$. In the proportional range, the stress-strain relationship for regular hexagonal lattices is given by $\sigma_{\infty} = 4\langle E \rangle/\sqrt{3}$ which, upon non-dimensionalisation, results in

$$\frac{\left(\overline{\sigma}_{\infty} \right)_{\text{Yield}}}{\langle \overline{\epsilon} \rangle_{\text{Yield}}} = \frac{4}{\sqrt{3}}, \tag{24}$$

whence $\langle \overline{\epsilon} \rangle_{\text{Yield}} = 1/(3\sqrt{3})$. Substituting this into (23), we obtain $\alpha = 2\sqrt{3}$. Thus we have an analytical response relationship for the lattice in terms of the beam defection function $G(x)$ as

$$\frac{3}{8} \overline{\sigma}_{\infty} = G\left(2\sqrt{3} \langle \overline{\epsilon} \rangle \right). \tag{25}$$

This curve is found to be very close to that obtained numerically (not shown for brevity), the difference being mainly attributable to the neglect of stretch deformation in the analysis.

The approach presented here is general with the potential for application to the response calculation of more complex lattice architectures. One of the important implications of equation (21) is that one is able to calculate the complete non-linear response of a complex elastic lattice which is bending dominated by carrying out a linear analysis, provided one is able to analytically calculate another point (but not the whole curve) on the $\overline{\sigma}_{\infty} - \langle \overline{\epsilon} \rangle$ relationship. One such

point is the onset of yield, as used above. Another possibility is that of the collapse point. The rest of the non-linear functionality is given by the function $G(x)$. In this manner, the argument developed in this section enables us to obtain analytical stress-strain curves for any lattice, in principle, as long as we are able to calculate certain identifiable points on the apparent stress-strain curve. Thus, we are able to separate the cell wall mechanics characterised via figure 12 from the kinematics of cell walls that depend on the lattice geometry. The two together afford the apparent stress-strain relationship such as the one above in equation (25).

Correspondence of points on the $\overline{P} - \overline{\delta}$ and the $\overline{\sigma}_\infty - \langle\overline{\epsilon}\rangle$ curves allows us to obtain other interesting pieces of information without extra effort. For example, equation (25) implies that the stress at collapse would given by $3(\overline{\sigma}_\infty)_{\text{Collapse}}/8 = 1/4$ and $2\sqrt{3}\langle\overline{\epsilon}\rangle_{\text{Collapse}} = 40/27$. The first of these for regular hexagonal lattices results in the well known formula for collapse [1] as $(\sigma_\infty)_{\text{Collapse}} = (2/3) \times \sigma_y t^2/l^2$, whereas the apparent strain at the point of collapse is given by

$$\langle\epsilon\rangle_{\text{Collapse}} = \left(\frac{20}{27\sqrt{3}}\right)\frac{\sigma_y l}{Et}, \tag{26}$$

a result not previously known. Note that the determination of the scale factors α or β did not make use of the collapse values on the $\overline{P} - \overline{\delta}$ curve. In spite of this, the corresponding values on the $\overline{\sigma}_\infty - \langle\overline{\epsilon}\rangle$ curve can now be predicted. Numerically obtained value of $\langle\epsilon\rangle_{\text{Collapse}} = 0.41$ agrees very favourably with the theoretically predicted one of $20/27\sqrt{3}$. Of course, these analytical formulas are approximate up to ignoring shear, axial strain, geometric non-linearity etc. as stated earlier. Also the analytical knowledge that strain at collapse scales linearly with the yield stress and the lattice characteristic length whereas it is inversely proportional to the Young's modulus and the cell wall thickness are very useful pieces of design information.

5. Conclusions

Honeycomb lattices are analysed here for plastic response and recoil starting from transition to plasticity up to collapse. The simplification of the cell wall mechanics using a beam idealisation coupled with lattice kinematics enables us to obtain analytical results. The underlying material behaviour is assumed to be elastic-perfectly-plastic which leads to a smooth apparent stress-strain relationship for the lattice.

The main contributions of the present work are summarised as follows. (a) A *benchmark analytical solution* for honeycomb plastic response was provided for the first time. Such problems have been studied computationally and experimentally before, but without any *analytical success*. (b) On the basis of the analytical framework developed in (a), we have obtained results, also analytically, for recoil of honeycombs post-plastic deformation. These calculations are not only theoretically significant, they are critical in many applications such as the assessment of recoil in stents. (c) The present work provides a framework to obtain *design sensitivities* analytically for a complex non-linear response. This are present in the dimensional groups used for the renormalisation of the apparent strain and the remote stress. (d) Scaling transformations that are non-trivial as they require physical arguments in addition to dimensional homogeneity, were developed successfully. This affords a '*non-linear master deformation profile*' –thus collapsing data for all the combinations of lattice and material parameters. (e) A separation of the non-linear mechanics of the cell wall and the lattice kinematics is achieved. This, together with the scaling transformations, enables response curves to be transformed to a single curve for various parametric changes. (f) The 'master curve' was fully characterised for critical points such as at transition to plasticity, collapse, relevant slope and shape, via non-dimensional numbers and non-dimensional functions describing shapes. (g) Using a kinematic argument, we show that the apparent Poisson's ratio of the honeycomb during plastic phase of deformation remains the same as that during the elastic phase. (h) Response of auxetic lattices under plastic deformation is

presented for the first time.

In summary, here we provide a benchmark analytical solution in the area of non-linear plastic response of hexagonal honeycombs with potential applications to a range of problems in applied mechanics, engineering and design. These could span from biomedical devices to crash and impact studies. Further work applied specifically to the design of cardiovascular stents will be presented elsewhere.

References

[1] L. J. Gibson, M. F. Ashby, Cellular solids: structure and properties, Cambridge university press, 1999.

[2] E. Tuncer, Numerical calculations of effective elastic properties of two cellular structures, Journal of Physics D: Applied Physics 38 (3) (2005) 497.

[3] V. Miranda, F. Teixeira-Dias, J. Pinho-da Cruz, F. Novo, The role of plastic deformation on the impact behaviour of high aspect ratio aluminium foam-filled sections, International Journal of Non-Linear Mechanics 45 (5) (2010) 550–561.

[4] H. Guoming, W. Hui, Z. Youlin, B. Wujun, A large deformation model for the elastic moduli of two-dimensional cellular materials, Journal of Wuhan University of Technology-Mater. Sci. Ed. 21 (2) (2006) 154–157.

[5] S. Malek, L. Gibson, Effective elastic properties of periodic hexagonal honeycombs, Mechanics of Materials 91 (2015) 226–240.

[6] H. Zhao, G. Gary, Crushing behaviour of aluminium honeycombs under impact loading, International Journal of Impact Engineering 21 (10) (1998) 827–836.

[7] H. Zhao, I. Elnasri, S. Abdennadher, An experimental study on the behaviour under impact loading of metallic cellular materials, International Journal of Mechanical Sciences 47 (4) (2005) 757–774.

[8] B. Haghpanah, J. Papadopoulos, D. Mousanezhad, H. Nayeb-Hashemi, A. Vaziri, Buckling of regular, chiral and hierarchical honeycombs under a general macroscopic stress state, in: Proc. R. Soc. A, Vol. 470, The Royal Society, 2014, p. 20130856.

[9] M. Paulino, F. Teixeira-Dias, An energy absorption performance index for cellular materials–development of a side-impact cork padding, International Journal of Crashworthiness 16 (2) (2011) 135–153.

[10] W. Goldsmith, J. L. Sackman, An experimental study of energy absorption in impact on sandwich plates, International Journal of Impact Engineering 12 (2) (1992) 241–262.

[11] F. A. El-Sayed, R. Jones, I. Burgess, A theoretical approach to the deformation of honeycomb based composite materials, Composites 10 (4) (1979) 209–214.

[12] C. B. Williams, J. K. Cochran, D. W. Rosen, Additive manufacturing of metallic cellular materials via three-dimensional printing, The International Journal of Advanced Manufacturing Technology 53 (1-4) (2011) 231–239.

[13] H. N. Wadley, Cellular metals manufacturing, Advanced Engineering Materials 4 (10) (2002) 726–733.

[14] G. Menges, F. Knipschild, Estimation of mechanical properties for rigid polyurethane foams, Polymer Engineering & Science 15 (8) (1975) 623–627.

[15] J. Klintworth, W. Stronge, Elasto-plastic yield limits and deformation laws for transversely crushed honeycombs, International Journal of Mechanical Sciences 30 (3) (1988) 273–292.

[16] H. Zhu, N. Mills, The in-plane non-linear compression of regular honeycombs, International Journal of Solids and Structures 37 (13) (2000) 1931–1949.

[17] D. Karagiozova, T. Yu, Plastic deformation modes of regular hexagonal honeycombs under in-plane biaxial compression, International journal of mechanical sciences 46 (10) (2004) 1489–1515.

[18] C.-H. Chuang, J.-S. Huang, Yield surfaces for hexagonal honeycombs with plateau borders under in-plane biaxial loads, Acta mechanica 159 (1-4) (2002) 157–172.

[19] A.-J. Wang, D. McDowell, Yield surfaces of various periodic metal honeycombs at intermediate relative density, International Journal of Plasticity 21 (2) (2005) 285–320.

[20] S. D. Papka, S. Kyriakides, In-plane compressive response and crushing of honeycomb, Journal of the Mechanics and Physics of Solids 42 (10) (1994) 1499–1532.

[21] S. D. Papka, S. Kyriakides, Experiments and full-scale numerical simulations of in-plane crushing of a honeycomb, Acta Materialia 46 (8) (1998) 2765–2776.

[22] C. Chen, T. Lu, N. Fleck, Effect of imperfections on the yielding of two-dimensional foams, Journal of the Mechanics and Physics of Solids 47 (11) (1999) 2235–2272.

[23] K. Mangipudi, S. Van Buuren, P. Onck, The microstructural origin of strain hardening in two-dimensional open-cell metal foams, International Journal of Solids and Structures 47 (16) (2010) 2081–2096.

[24] L. Gibson, M. Ashby, G. Schajer, C. Robertson, The mechanics of two-dimensional cellular materials, in: Proceedings of the Royal Society of London A: Mathematical, Physical and Engineering Sciences, Vol. 382, The Royal Society, 1982, pp. 25–42.

[25] S. Pellegrino, C. R. Calladine, Matrix analysis of statically and kinematically indeterminate frameworks, International Journal of Solids and Structures 22 (4) (1986) 409–428.

[26] T. Yu, W. Johnson, Influence of axial force on the elastic-plastic bending and springback of a beam, Journal of Mechanical Working Technology 6 (1) (1982) 5–21.

[27] A. Bhaskar, The effective poisson ratio of random cellular matter having bending dominated architecture, EPL (Europhysics Letters) 87 (1) (2009) 18004.

[28] G. I. Barenblatt, Scaling, self-similarity, and intermediate asymptotics: dimensional analysis and intermediate asymptotics, Vol. 14, Cambridge University Press, 1996.

[29] G. Taylor, The formation of a blast wave by a very intense explosion. i. theoretical discussion, Proceedings of the Royal Society of London. Series A, Mathematical and Physical Sciences 201 (1065) (1950) 159–174.

[30] G. N. Greaves, A. Greer, R. Lakes, T. Rouxel, Poisson's ratio and modern materials, Nature materials 10 (11) (2011) 823–837.

[31] R. Lakes, Materials science: A broader view of membranes, Nature 414 (6863) (2001) 503–504.

[32] M. Warner, B. Thiel, A. Donald, The elasticity and failure of fluid-filled cellular solids: theory and experiment, Proceedings of the National Academy of Sciences 97 (4) (2000) 1370–1375.